HHS Public Access

Author manuscript

Cell Res. Author manuscript; available in PMC 2011 March 01.

Published in final edited form as:

Cell Res. 2010 September ; 20(9): 1012–1022. doi:10.1038/cr.2010.93.

Organ-specific enhancement of metastasis by spontaneous ploidy duplication and cell size enlargement

Xin Lu[1], **Xuemin Lu**[1], and **Yibin Kang**[1,2,3]

[1]Department of Molecular Biology, Princeton University, Princeton, NJ 08544, USA

[2]Breast Cancer Program, The Cancer Institute of New Jersey, New Brunswick, NJ 08903, USA

Abstract

Aneuploidy is commonly observed in breast cancer and is associated with poor prognosis. One frequent type of aneuploidy, hypertetraploidy, may derive from ploidy duplication of hyperdiploid cells. However, the pathological consequences of ploidy duplication in breast cancer progression have not been characterized. Here, we present an experimental system demonstrating spontaneous appearance of hypertetraploid cells from organ-specific metastatic variants of the MDA-MB-231 breast cancer cell line through ploidy duplication *in vitro* and *in vivo*. The hypertetraploid progenies showed increased metastatic potential to lung and brain, but not to bone, which may be partially explained by the distinct capillary structures in these organs that confer differential lodging advantages to tumor cells with enlarged size. Our results suggest a potential mechanistic link between ploidy duplication and enhancement of metastatic potentials, as was observed in previous clinical studies of breast cancer.

Keywords

breast cancer; metastasis; organotropism; hyperploidy; cell size

Introduction

Malignant spread of cancer cells, or metastasis, accounts for the majority of cancer-related mortality [1, 2]. Better molecular and cellular understanding of the multi-step metastasis cascade holds promise to control this dreadful disease. As one of the hallmarks of malignant cancer cells, aneuploidy is frequently observed in a large variety of cancer types and is associated with poor prognosis [3]. Several types of aneuploidy exist, including hypodiploidy, hyperdiploidy, hypertetraploidy and multiploidy. In breast adenocarcinoma, patients with hypertetraploid, hypodiploid and multiploid tumors had worse prognosis than those with diploid and hyperdiploid tumors [4], with hypertetraploid tumors being the most

[3]To Whom Correspondence should be addressed. Yibin Kang, Ph.D, Department of Molecular Biology, Washington Road, LTL 255, Princeton University, Princeton, NJ 08544, Phone:+01-609-258-8834; Fax: +1-609-258-2340; ykang@princeton.edu.

Competing Financial Interests

The authors declare no competing financial interests.

aggressive ones in some reports [5]. Hypertetraploidy was hypothesized to derive from endoreduplication of hyperdiploid cells during breast cancer progression [6]. Alternatively, hypertetraploidy may arise as a consequence of cell fusion, which occurs in higher frequencies in inflamed tissues and tumors [7, 8]. Hypertetraploid tumor cells typically have increased nuclear and cell size [9]. The increase of nuclear dimension during cancer progression has been shown to associated with poor clinical outcomes in many different types of malignancies, such as breast cancer [10-12], prostate cancer [13, 14], and melanoma [15]. In particular, increased nuclear area was found to have strong correlations with advanced tumor stage, poor survival and increased risk of metastasis in breast cancer [10]. However, without a suitable experimental model system that recapitulates spontaneous formation of hypertetraploidy tumor cells, the pathological consequences of hypertetraploidy remains poorly understood. Here, we present a model system for the spontaneous *in vitro* and *in vivo* derivation of hypertetraploid tumor cells from different metastatic variants of the MDA-MB-231 breast cancer cell line. We compared the cellular and molecular characteristics of hypertetraploid breast cancer cells with their hyperdiploid parental counterparts. Furthermore, through extensive evaluation of their *in vivo* metastatic behaviors, we linked the enhanced metastatic potential of hypertetraploid tumor cells to lung and brain with the specialized blood vessel structures in these organs. Our study established a model system to analyze the impact of spontaneous ploidy duplication on tumor progression and metastasis and provided novel mechanistic insights for the organ-specific enhancement of metastatic abilities of hypertetraploid tumor cells.

Results

Spontaneous formation of hypertetraploidy from hyperdiploid tumor cells

Two organotropic metastatic variants of the MDA-MB-231 human breast cancer cell line [2]—the lung-metastatic LM2 [16] and the bone-metastatic1833 (re-named as BM1 in the current study to facilitate presentation) [17]—were passaged for nearly one year *in vitro* to evaluate the relative genomic and phenotypic stability of organ-specific metastatic cell lines. Weekly DNA content analysis revealed a surprising ploidy pattern shift for both lines (Figure 1A). Predominant 2N/4N peaks (N= haploidy of parental MDA-MB-231) were gradually replaced by one peak slightly lower than 4N and another peak close to 8N. Apparently, the original cell lines were re-populated by cells with approximately doubled DNA content. The three peaks were very obvious during the transition (i.e. between week 21 and week 25 in Figure 1A) with the middle peak (close to 4N) composed of the G2/M peak of the original (hyperdiploid) population and the G1/G0 peak of the newly evolved population (hypertetraploid). Such a mixed ploidy profile closely resembles the clinical observation of multiploidy in a subset of breast cancer patients [4], suggesting that multiploidy may be the transitional state between hyperdiploidy and hypertetraploidy. The genetic continuity of the two populations with distinct ploid levels presented us with a unique opportunity to investigate the potential functional consequence of spontaneous ploidy duplication in malignant phenotypes.

To isolate the two closely matched and relatively pure sub-populations of hyperdiploid and hypertetraploid cells from the same cell line, we stained the cells at the multiploidy stage

with Hoechst 33342 and sorted the G1/G0 peak of the hyperdiploid population (termed "modal") and the G2/M peak of the hypertetraploid population (termed "hyper") (Figure 1B). Spectral karyotyping determined the average chromosome numbers for LM2-modal, LM2-hyper, BM1-modal and BM1-hyper to be 61, 103, 56 and 107, respectively (Figure 2A-B). The hyper cells adopted all major chromosomal aberrations of the parental modal cells, although a small number of new abnormalities also evolved (Figure 2C-D). Nearly doubled chromosomes and highly conserved chromosomal structures suggest the hyper cells were indeed derived from the chromosomal complement duplication from the modal cells [6, 9], and ruled out the possibility that the appearance of the hypertetraploid population during long-term culture was due to the outgrowth of a contaminated population distinct from MDA-MB-231. The proliferation rates of the hyper cells were nearly identical to the corresponding modal cells in culture (Figure 3A). The comparable growth rates and tumor characteristics were also observed *in vivo* (Figure 3B-C), indicating that ploidy change did not significantly change tumor proliferation, at least during the time window of the *in vitro* and *in vivo* tumor growth experiments.

Organ-specific promotion of metastasis by ploidy duplication

Since hypertetraploidy has been previously linked to poor clinical outcomes, we evaluated the potential contribution of ploidy duplication to metastasis development. Modal and hyper derivatives of LM2 and BM1 were subjected to *in vivo* lung metastasis and bone metastasis assays, respectively. We were also able to test brain metastasis as LM2 cells showed mild brain-metastatic ability, consistent with the finding that genes mediating lung-metastasis and brain metastasis partially overlapped [18]. All cells were labeled with a dual reporter expressing *renilla* luciferase and mRFP to facilitate bioluminescence imaging (BLI) and fluorescence imaging [19]. Intriguingly, differential metastatic behavior alterations were observed in different organs when hyper and modal cells were compared. In lung and brain, LM2-hyper caused significantly more metastasis burden than LM2-modal (Figure 4A-D). The increased metastasis burden detected by BLI (Figure 4A and 4C) were further confirmed by necropsy and H&E staining of metastatic lesions (Figure 4B and 4D). In contrast, BM1-modal and BM1-hyper showed no difference in colonizing the bone (Figure 4E). X-radiography and Goldner's trichromse staining showed similar degree of metastasis-associated osteolysis in the tibia (Figure 4F). The absence of enhanced metastatic potential to bone by BM1-hyper was not due to the optimal bone-metastatic ability that already exists in BM1-modal, because LM2-hyper, derived from the weakly bone-metastatic LM2-modal, also failed to display more metastatic potential to bone (data not shown).

DNA content analysis of freshly isolated metastases formed by LM2 or BM1 indicated that spontaneous ploidy duplication also occurred *in vivo* (Figure 5A-B), ruling out the possibility that the process was simply an *in vitro* artifact. Metastases formed by LM2-hyper and BM1-hyper showed stably maintained hypertetraploid DNA composition (Figure 5C-D), confirming that the phenotypic changes were caused by the ploidy doubling.

Lack of transcriptomic changes due to ploidy duplication

To explain the organ-specific enhancement of metastasis by ploidy duplication, we determined whether ploidy evolution differentially influenced the expression of genes

important for organotropic metastasis. Previously identified bone-, lung- and brain-specific metastasis gene signatures using the MDA-MB-231 system [16-18] were used to cluster modal and hyper cells as well as other MDA-MB-231 sublines with well-defined metastatic abilities [16-18] (Figure 6A-C). Surprisingly, LM2-modal and LM2-hyper always clustered together, as is the case with BM1-modal and BM1-hyper. Ploidy duplication neither shifted the expression profile of a weakly metastatic cell to that of a highly metastatic one, nor obviously changed the expression levels of signature genes for highly metastatic cells. These notions were further supported by Gene Set Enrichment Analysis [20, 21], which failed to find enrichment of either of the three signatures in hyper cells (see Materials and Methods for details). When LM2- and BM1-modal were compared with LM2- and BM-hyper to identify any ploidy-regulated gene(s), no such gene(s) could be found by statistical analysis (see Materials and Methods). Such findings may not be entirely unexpected if one considers the resistance of gene expression alteration to ploidy changes in yeast [22]. The absence of ploidy-regulated genes in our current study reflects the robustness of transcriptome when all (or most) genetic materials are synchronously duplicated.

Enhanced organ-specific metastasis abilities linked to cell size enlargement

Increased cell size is a conspicuous consequence of increased ploidy in yeast, plant and mammalian cells [9]. We observed an approximately 1.5-fold increase of cell volume of hyper cells (Figure 7A-B). Biophysical properties of circulating tumor cells, including adhesiveness, rigidity and size, were associated with metastatic ability in previous studies [23-25]. Therefore, we wanted to determine whether enlarged cell size by ploidy alteration might play any role in causing the organotropic enhancement of metastasis. Lodging of tumor cells within 12h of inoculation in three organs were evaluated by fluorescence imaging of labeled tumor cells. In lung and brain, most tumor cells were within the capillaries, whereas in bone, most were located outside of vasculature (Figure 7C-D). Interestingly, there were significantly more LM2-hyper cells than LM2-modal cells arrested in the capillaries of lung and brain, whereas BM1-modal and BM1-hyper showed similar lodging efficiency in the bone marrow (Figure 7E). Recently, the structural feature of capillary walls in different organs was recognized as an important factor to affect tumor cell infiltration [26]. While the fenestrated structure of bone marrow sinusoid capillaries may be permissive to circulating tumor cells, the continuous endothelium in the lung and the tight blood-brain barrier in the brain could readily arrest tumor cells with size larger than the capillary diameter and only allow extravasation if the cells possess molecular properties that facilitate the penetration of vascular structures. Linking this finding to our current observations, we concluded that the enlarged cell size caused by ploidy duplication may result in more metastatic arrest of tumor cells only in the capillaries non-permissive to free cell trafficking (i.e. those in the lung and brain). In comparison, increase in cell size may not affect tumor cell infiltration through the fenestrated bone marrow capillaries.

Discussion

Hematogenous metastasis is a multi-step process involving complex tumor-stroma interactions [1]. Most of the current efforts of metastasis research focus on the identification of genes and signaling pathways that mediate metastasis with an emphasis on the organ-

specific functions of the molecular mediators [1, 27]. These efforts strived to understand the biochemical compatibility of tumor and stroma during metastasis and have successfully extend the concept of the “seed” and “soil” hypothesis into molecular levels [28]. However, another potentially important aspect of the “seed” and “soil” hypothesis, the biophysical compatibility between tumor cells and target organs, has been largely overlooked in the modern era of metastasis research. Systemic dissemination of tumor cell is not a random process. Instead, physical properties of tumor cells can influence the efficiency of the arrest and seeding in secondary organs. In the present study, by investigating the organ-specific metastasis behaviors of hypertetraploid cells and their isogenic hyperdiploid counterparts, we found enlarged cell size confers a quantitative advantage when lodging at organs with continuous vasculature (i.e. lung and brain), but not in organ that have fenestrated capillaries (bone). This result is in line with a recent study suggesting that organ-specific vascular structures accounted for the selective advantages of TGFβ-induced Angptl4 to promote lung metastasis but not bone metastasis [29]. The correlation between larger cell size with increased efficiency of metastatic seeding was also observed in a recent study using intravital real-time imaging of lung metastasis seeding and progression [30]. However, we could not rule other possible mechanisms that could also account for the increased lung and brain metastasis by LM2-hyper cells. For example, hypertetraploid cells may be more resistant to rapid apoptosis after initial arrest compared with hyperdiploid cells in lung and brain, but not in bone, although the mechanism of organ specificity of apoptosis behavior changes by ploidy duplication is elusive.

It is obvious that enlarged cell size by ploidy duplication is not necessary for metastasis to occur; for example, LM2-modal is already highly metastatic to lung. BM1-modal is essentially non-metastatic to lung [16]. If enlarged cell size were sufficient to confer metastasis ability to lung, we would expect BM1-hyper became lung-metastatic. Our preliminary experiments indicated that BM1-hyper, similar to BM1-modal, was still not able to form lung metastasis (data not shown). This finding indicates that the cell size increase as a consequence of ploidy shift is by itself not sufficient to enable lung metastasis formation. Taken together, the increased cell size only serves as a biophysical modulator of the metastasis ability. Gene expression pattern and biochemical activity of tumor cells still play a dominant role in determining the metastatic potential and organ specificity of malignant tumor cells. Indeed, the most likely reason for the inability of BM1-modal and BM1-hyper cells to colonize the lung is the lack of essential genes for lung metastasis, such as *ANGPTL4, EREG and COX2* [1, 16, 29].

The enlarged cell size is a consequence of ploidy duplication, as observed in our study. Ploidy duplication, or polyploidy in general, has profound influence during evolution [9] as well as cancer progression. Tetraploidy caused by cykokinesis failure promoted tumorigenesis [9] and was proposed as an intermediate stage for cancer aneuploidy during the early stages of tumorigenesis [9]. It should be noted that MDA-MB-231 is already aneuploid before any experimental handling. The ploidy shift studied here was the transition from hyperdiploidy (one type of aneuploidy) to hypertetraploidy (another type of aneuploidy). Ploidy duplication may lead to chromosome reshuffling and massive instability. However, our observation indicated that the hypertetraploid descendants were

genetically stable, consistent with our previously reported finding that tumor-tumor cell fusion in MDA-MB-231 generated stable hybrids [19]. The genetic stability is possibly linked to the ability of supernumerary centrosomes to cluster into two functional mitotic spindles in advanced malignant cells [19]. The similarity of genomic stability between hypertetraploid cells and cells derived from fusion of MDA-MB-231 cells [19] raises the possibility that cell fusion may initiate ploidy duplication. Alternatively, endoreduplication as the result of cytokinesis failure or mitotic slippage can also lead to chromosome doubling [31]. During the course of our study, we observed that not all MDA-MB-231 derived cells were able to spontaneously progress to higher ploidy after extensive period of cell culture. Another MDA-MB-231 subline, SCP2, did not progress to higher ploidy when cultured for nearly one year. Since both SCP2 and LM2 undergo spontaneous cell fusion at a low frequency [19], yet only LM2 could undergo massive ploidy duplication, endoreduplication instead of cell fusion is more likely to be the cause of ploidy shift in our current experimental system. Nevertheless, the exact cellular and molecular mechanism of ploidy duplication remains obscure and should be further investigated.

Overall, results from this study suggest that metastasis is not simply a metastasis gene-driven event, but also a process subjected to influence by the biophysical properties of the constantly evolving tumor cells. Importantly, our study provided a direct mechanistic explanation for the previous clinical observations that hypertetraploidy and enlarged nuclear size are linked to poor survival and metastasis [5, 10-12]. In addition, the model system established in our study may become a useful platform for functional studies of putative molecular mediators of ploidy duplication, which could be explored as potential new targets for prophylactic cancer therapy to prevent metastasis. Further efforts should investigate the generality of these findings in breast as well as other types of cancer and explore the clinical association of hyperploidy with organ-specific metastases.

Materials and Methods

Cell culture

LM2 (4175) [16], BM1 (1833) [19] and their sublines were maintained in DMEM with10% FBS and antibiotics.

Flow cytometry, spectral karyotyping and cell volume measurement

DNA content analysis and sorting with propidium iodide staining, Hoechst 33342 staining and subsequent flow cytometry were performed as described [19]. Spectral karyotyping was performed by the SKY/FISH facility in the Roswell Park Cancer Institute as described [19]. Cell volume was measured with a Coulter counter as described [19].

In vitro growth curve

Cells (2×10^4) were seeded into 6-well plates with 3 wells / cell line/ time point. Medium was changed every 2 days. Cells were counted every 2 days.

Tumor xenografts and analysis

All procedures involving mice, such as housing and care, and all experimental protocols were approved by Institutional Animal Care and Use Committee (IACUC) of Princeton University. For intracardiac injections to generate bone and brain metastases, 10^5 cells in PBS were injected into the left cardiac ventricle of 4-week-old, female nude mice (NCI) as described [17, 18, 32]. For intravenous injection to generate lung metastases, 2×10^5 cells in PBS were injected into the tail vein of nude mice as described [16]. Development of metastases in bone and lung was monitored by BLI with the IVIS Imaging System (Xenogen) as described [16, 17]. BLI analysis was performed with Living Image software (Xenogen) by measuring photon flux of the region of interest. X-ray radiography analysis of bone lesions was performed using procedures as described [17]. For the orthotopic xenograft model, mammary fat pad injections and tumor size measurements were performed as described [16, 32].

Histological and fluorescence analyses

Hindlimb bone, lung and brain were excised, fixed in 10% neutral-buffered formalin, decalcified (for bone only), and embedded in paraffin for hematoxylin and eosin (H&E) staining or Goldner's trichromse staining [33]. Immunofluorescent staining of microtubules was performed with mouse anti-α tubulin (Sigma) primary antibody and Alexa Fluor 568-conjugated secondary antibody. Actin was stained with Alexa Fluor 488-conjugated phalloidin. To study the tumor cell arrest in different organs, tumor cells were labeled with the green-fluorescent vital dye CFDA SE Cell Tracer (Invitrogen) following the manufacturer's instruction. The inherent mRFP label was lost during the tissue fixation step, and therefore could not be used for tracing the cells. Tumor cells were injected into nude mice. Twelve hours later, mice were injected with 1mg/mouse of Texas Red-conjugated dextran (70,000 MW, Invitrogen) 10 minutes before sacrifice to label blood vessels. Lung, brain and bone were fixed with cold 10% formalin, decalcified (for bone only), and embedded in OCT for frozen sectioning (10μm/section) and fluorescence imaging. Tumor cells were quantified as number/field for lung and brain and converted to number/mm^2. For bone, because tumor cells were sparse, they were expressed as total number/hindlimb (femur and tibia) based on calculations of 20 sections (200μm in total) and the thickness of the bone cavity (approximately 1mm).

DNA content analysis of primary metastasis lesions from mice

Small pieces of lung with multiple metastasis nodules were minced and digested as described [34]. Femur or tibia with metastatic lesions was flushed as described [35]. Red blood cells were lysed with ACK lysis buffer [36]. Cells were fixed immediately or briefly cultured overnight before fixation and subjected to DNA content analysis as described [19].

Microarray analysis

The same procedure as previously described [17] was used to conduct the microarray experiments for LM2-modal, LM2-hyper, BM1-modal and BM1-hyper on the Affymetrix U133A chips. Data were deposited at the NCBI Gene Expression Omnibus (http://www.ncbi.nlm.nih.gov/geo/) with the accession GSE16554. Hierarchical clustering was

performed with the Genespring GX 7.3 software (Agilent Technologies) using the organ-specific metastasis gene signatures and associated cell line microarray data [16-18]. To identify ploidy-regulated gene(s), four cell lines were separated into the modal group containing LM2- and BM1-modal and the hyper group containing LM2-and BM1-hyper. ANOVA was used to find genes with significant difference between two groups with Genespring GX 7.3 software (Agilent Technologies) using following conditions: pamametric test, do not assume equal variance; FDR 0.05; Multiple testing correction Benjamini and Hochberg FDR. GSEA software [20, 37] was used to analyze the enrichment for the following gene sets: up-regulated and down-regulated subsets of the lung metastasis signature [16], up-regulated and down-regulated subsets of the bone metastasis signature [17], up-regulated and down-regulated subsets of the genes associated with brain metastatic behavior [18]. False Discovery Rate (FDR) cutoff of 0.25 was used as criterion of statistical significance as recommended.

Statistical analysis

Results were reported as average ± s.d. (standard deviation) or s.e.m. (standard error of the mean), indicated in the figure legends. Comparisons were performed using unpaired two-sided Student's t-test without equal variance assumption or nonparametric Mann-Whitney test.

Acknowledgements

We thank M. Yuan and M. Bisher for assistance with histology; C. DeCoste for assistance with flow cytometry. Y.K. is a Champalimaud Investigator and a Department of Defense Era of Hope Scholar Award recipient. This research was additionally supported by grants from the National Institutes of Health (R01CA134519), the American Cancer Society, the Susan G. Komen for the Cure and the New Jersey Commission on Cancer Research. Xin Lu is a recipient of a Harold W. Dodds Fellowship from Princeton University.

References

1. Gupta GP, Massague J. Cancer metastasis: building a framework. Cell. 2006; 127:679–695. [PubMed: 17110329]
2. Lu X, Kang Y. Organotropism of Breast Cancer Metastasis. Journal of Mammary Gland Biology and Neoplasia. 2007; 12:153–162. [PubMed: 17566854]
3. Rajagopalan H, Lengauer C. Aneuploidy and cancer. 2004; 432:338–341.
4. Coulson P, Thornthwaite J, Woolley T, Sugarbaker E, Seckinger D. Prognostic indicators including DNA histogram type, receptor content, and staging related to human breast cancer patient survival. Cancer research. 1984; 44:4187–4196. [PubMed: 6744328]
5. Kallioniemi OP, Blanco G, Alavaikko M, et al. Improving the prognostic value of DNA flow cytometry in breast cancer by combining DNA index and S-phase fraction. A proposed classification of DNA histograms in breast cancer. Cancer. 1988; 62:2183–2190. [PubMed: 3179930]
6. Dutrillaux B, Gerbault-Seureau M, Remvikos Y, Zafrani B, Prieur M. Breast cancer genetic evolution: I. Data from cytogenetics and DNA content. Breast Cancer Research and Treatment. 1991; 19:245–255. [PubMed: 1663804]
7. Lu X, Kang Y. Cell fusion as a hidden force in tumor progression. Cancer Res. 2009; 69:8536–8539. [PubMed: 19887616]
8. Singec I, Snyder EY. Inflammation as a matchmaker: revisiting cell fusion. Nature cell biology. 2008; 10:503–505. [PubMed: 18454127]

9. Storchova Z, Pellman D. FROM POLYPLOIDY TO ANEUPLOIDY, GENOME INSTABILITY AND CANCER. Nature Reviews Molecular Cell Biology. 2004; 5:45–54. [PubMed: 14708009]
10. Abdalla F, Boder J, Markus R, Hashmi H, Buhmeida A, Collan Y. Correlation of nuclear morphometry of breast cancer in histological sections with clinicopathological features and prognosis. Anticancer research. 2009; 29:1771–1776. [PubMed: 19443402]
11. van Bogaert LJ, de Muylder C, Maldague P, Maisin H. Prognostic implications of mean nuclear diameter in breast cancer. British journal of cancer. 1980; 42:537–541. [PubMed: 7437288]
12. Zajdela A, De LaRiva LS, Ghossein NA. The relation of prognosis to the nuclear diameter of breast cancer cells obtained by cytologic aspiration. Acta cytologica. 1979; 23:75–80. [PubMed: 285555]
13. Khan MA, Walsh PC, Miller MC, et al. Quantitative alterations in nuclear structure predict prostate carcinoma distant metastasis and death in men with biochemical recurrence after radical prostatectomy. Cancer. 2003; 98:2583–2591. [PubMed: 14669277]
14. Blom JH, Ten Kate FJ, Schroeder FH, van der Heul RO. Morphometrically estimated variation in nuclear size. A useful tool in grading prostatic cancer. Urological research. 1990; 18:93–99. [PubMed: 2187298]
15. Mossbacher U, Knollmayer S, Binder M, Steiner A, Wolff K, Pehamberger H. Increased nuclear volume in metastasizing “thick” melanomas. The Journal of investigative dermatology. 1996; 106:437–440. [PubMed: 8648173]
16. Minn AJ, Gupta GP, Siegel PM, et al. Genes that mediate breast cancer metastasis to lung. Nature. 2005; 436:518–524. [PubMed: 16049480]
17. Kang Y, Siegel PM, Shu W, et al. A multigenic program mediating breast cancer metastasis to bone. Cancer Cell. 2003; 3:537–549. [PubMed: 12842083]
18. Bos PD, Zhang XHF, Nadal C, et al. Genes that mediate breast cancer metastasis to the brain. Nature. 2009; 459:1005–1009. [PubMed: 19421193]
19. Lu X, Kang Y. Efficient acquisition of dual metastasis organotropism to bone and lung through stable spontaneous fusion between MDA-MB-231 variants. Proceedings of the National Academy of Sciences. 2009; 106:9385–9390.
20. Subramanian A, Tamayo P, Mootha VK, et al. Gene set enrichment analysis: A knowledge-based approach for interpreting genome-wide expression profiles. Proceedings of the National Academy of Sciences of the United States of America. 2005; 102:15545–15550. [PubMed: 16199517]
21. Mootha VK, Lindgren CM, Eriksson KF, et al. PGC-1alpha-responsive genes involved in oxidative phosphorylation are coordinately downregulated in human diabetes. Nat Genet. 2003; 34:267–273. [PubMed: 12808457]
22. Galitski T, Saldanha AJ, Styles CA, Lander ES, Fink GR. Ploidy Regulation of Gene Expression. Science. 1999; 285:251–254. 10.1126/science.285.5425.251. [PubMed: 10398601]
23. Watanabe S. The metastasizability of tumor cells. Cancer. 1954; 7:215–223. [PubMed: 13141212]
24. Zeidman I. The Fate of Circulating Tumor Cells: I. Passage of Cells through Capillaries. Cancer Research. 1961; 21:38–39. [PubMed: 13788099]
25. Koike A. Mechanism of Blood-Borne Metastases. I. Some Factors Affecting Lodgment and Growth of Tumor Cells in the Lungs. Cancer. 1964; 17:450–460. [PubMed: 14136528]
26. Nguyen DX, Bos PD, Massague J. Metastasis: from dissemination to organ-specific colonization. Nat Rev Cancer. 2009; 9:274–284. [PubMed: 19308067]
27. Kang Y. Functional genomic analysis of cancer metastasis: biologic insights and clinical implications. Expert review of molecular diagnostics. 2005; 5:385–395. [PubMed: 15934815]
28. Paget S. Distribution of secondary growths in cancer of the breast. Lancet. 1889; 1:571–573.
29. Padua D, Zhang XH, Wang Q, et al. TGFbeta primes breast tumors for lung metastasis seeding through angiopoietin-like 4. Cell. 2008; 133:66–77. [PubMed: 18394990]
30. Kimura H, Hayashi K, Yamauchi K, et al. Real-time imaging of single cancer-cell dynamics of lung metastasis. J Cell Biochem. 2010; 109:58–64. [PubMed: 19911396]
31. Ganem NJ, Storchova Z, Pellman D. Tetraploidy, aneuploidy and cancer. Current opinion in genetics & development. 2007; 17:157–162. [PubMed: 17324569]

32. Kang Y. Analysis of cancer stem cell metastasis in xenograft animal models. Methods in molecular biology (Clifton, NJ. 2009; 568:7–19.

33. Lu X, Kang Y. Chemokine (C-C motif) ligand 2 engages CCR2+ stromal cells of monocytic origin to promote breast cancer metastasis to lung and bone. The Journal of biological chemistry. 2009; 284:29087–29096. [PubMed: 19720836]

34. Yang J, Mani SA, Donaher JL, et al. Twist, a master regulator of morphogenesis, plays an essential role in tumor metastasis. Cell. 2004; 117:927–939. [PubMed: 15210113]

35. Lu X, Wang Q, Hu G, et al. ADAMTS1 and MMP1 proteolytically engage EGF-like ligands in an osteolytic signaling cascade for bone metastasis. Genes & Development. 2009; 23:1882–1894. [PubMed: 19608765]

36. Sauer KA, Scholtes P, Karwot R, Finotto S. Isolation of CD4+ T cells from murine lungs: a method to analyze ongoing immune responses in the lung. Nat Protocols. 2007; 1:2870–2875. [PubMed: 17406546]

37. Mootha VK, Lindgren CM, Eriksson K-F, et al. PGC-1[alpha]-responsive genes involved in oxidative phosphorylation are coordinately downregulated in human diabetes. Nat Genet. 2003; 34:267–273. [PubMed: 12808457]

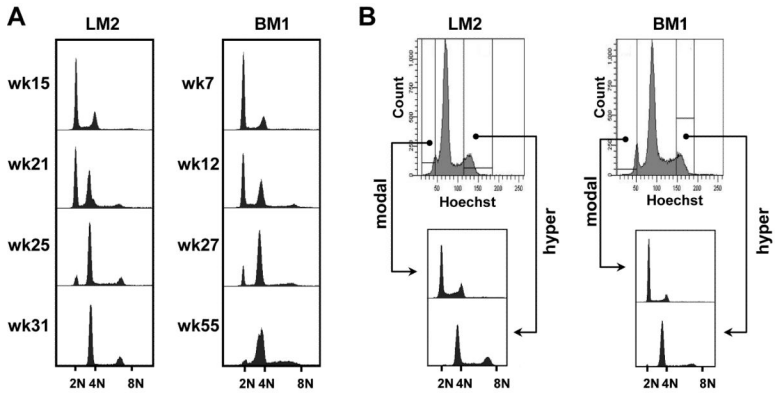

Figure 1.

Spontaneous ploidy duplication generated hypertetraploid cells. **(A)** DNA content evolution of *in vitro* cultured LM2 and BM1 during long term cell culture. Flow cytometry DNA content profiles of cells collected at the indicated time point during long term cell culture are shown. **(B)** Sorting of modal and hyper cells during the ploidy transition period after the cells were labeled with vital DNA dye Hoechst 33342. N = haploidy of the parent MDA-MB-231 cell line.

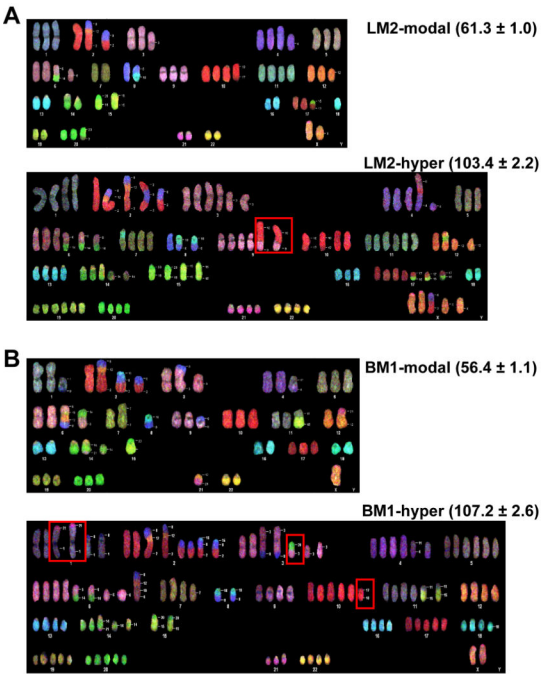

C

Marker Chr.	LM2-modal	LM2-hyper
t(2;8)	+	+
t(2;12;8)	+	+
del(3)	+	+
del(6)	+	+
t(6;14)	+	+
t(8;18)	+	+
t(10;17)	+	+
del(12)	+	+
t(15;15)	+	+
t(15;17)	+	+
t(15;20)	+	+
t(17;20)	+	+
del(X)	+	+
t(9;10)	-	+
del(14)	-	+

D

Marker Chr.	BM1-modal	BM1-hyper
t(1;8)	+	+
t(2;8)	+	+
t(2;8;16)	+	+
t(2;12;8)	+	+
del(3)	+	+
t(3;8)	+	+
t(4;11)	+	+
t(6;14)	+	+
t(6;19;12;8)	+	+
t(8;18)	+	+
t(11;15)	+	+
del(14)	+	+
t(14;21)	+	+
t(15;20)	+	+
t(1;21)	-	+
t(3;20)	-	+
del(6)	-	+
t(10;17)	-	+
t(x;4)	-	+

Figure 2.

Hypertetraploid (hyper) cells inherited the majority of the chromosomes with characteristic abnormalities (marker chromosomes) from the hyperdiploid (modal) cells. **(A-B)** Representative spectral karyotyping images showing the chromosomal composition of each cell line. Total chromosome number was indicated as average ± s.d. with 20 metaphase spreads counted. Red squares indicate the newly evolved chromosome aberrations. **(C-D)** Summary of marker chromosomal translocations and deletions identified in the indicated cell lines.

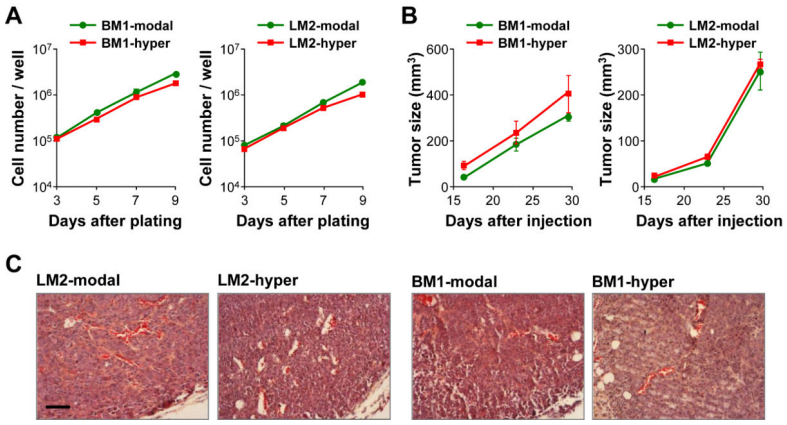

Figure 3.

Similar growth rates of modal and hyper cells *in vitro* and *in vivo*. **(A)** *In vitro* growth curves showing similar growth rates of modal and hyper cells, for either BM1 or LM2, during the exponential growth phase. Data represent average ± s.d. with triplicate for each line at each time point. **(B)** Tumor growth curves at the mammary glands with similar slopes across all time points suggesting similar growth rates of modal and hyper cells, for both BM1 or LM2. Data represent average ± s.e.m. n = 6 tumors/group. **(C)** H&E staining of respective tumors. Scale bar represents 100μm.

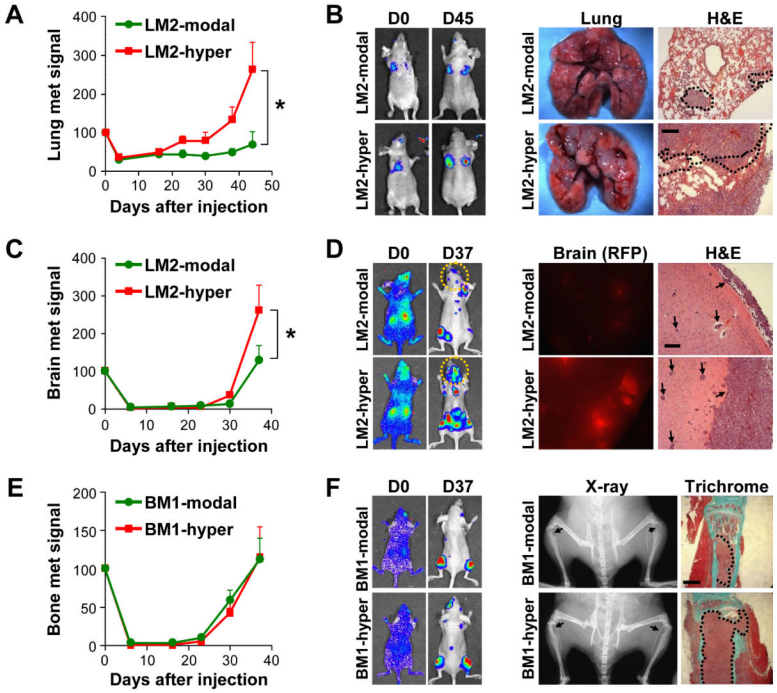

Figure 4.

Ploidy duplication enhanced metastasis to lung and brain, but not to bone. **(A)** Metastasis burden quantified by bioluminescence imaging (BLI) at different time points after intravenous tumor cell injection showed that LM2-hyper was more metastatic to lung than LM2-modal, with representative mice, fresh lung tissue and H&E staining shown in **(B)**. **(C)** LM2-hyper was more metastatic to brain than LM2-modal after intracardiac injection, with representative mice, fresh brain tissue with fluorescent stereoscopy and H&E staining shown in **(D)**. **(E)** BM1-hyper and BM1-modal showed similar metastatic ability to bone after intracardiac injection, with representative mice, X-ray radiographs and Goldner's trichrome staining shown in **(F)**. In **A**, **C** and **E**, error bar represents s.e.m. n= 8 mice/group. (*) $P<0.05$ with Mann-Whitney test. In **B**, **D** and **F**, major metastases were indicated by dotted contour line or arrow. Scale bars represent 200 μm in **B** and **D**, 800 μm in **F**.

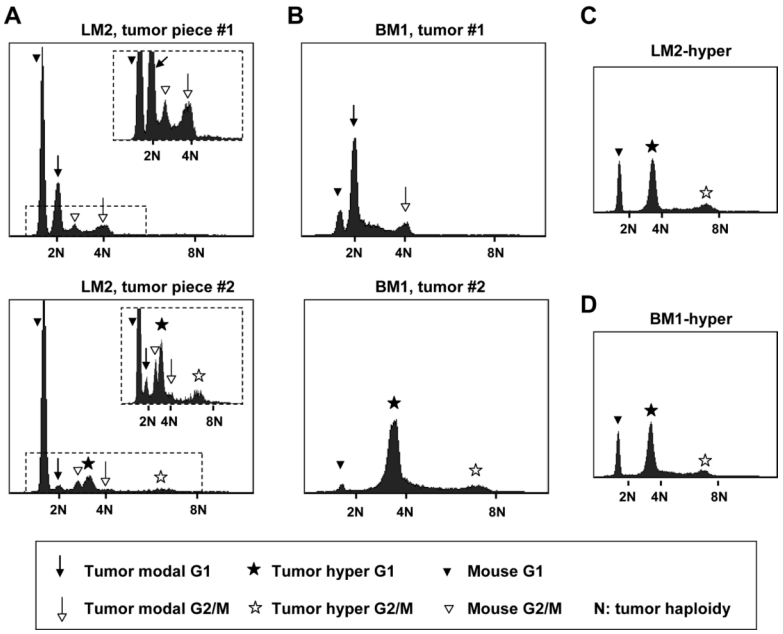

Figure 5.

Spontaneous ploidy duplication and stable DNA content of hypertetraploid cells during *in vivo* metastasis progression. **(A)** Two representative lung pieces with multiple metastasis nodules formed after intravenous injection of LM2 cells. Tumor #1 represents predominantly maintained hyperdiploidy of tumor cells in the nodules, while tumor #2 represents partially converted ploidy from hyperdiploidy to hypertetraploidy in the nodules One out of 3 lung pieces contained detectable hypertetraploid nodules. Inserts show the enlarged areas of the DNA content profiles. **(B)** Two representative bone marrow flushes with metastases formed after intracardiac injection of BM1 cells. Tumor #1 represents fully maintained hyperdiploidy of tumor cells, while tumor #2 represents almost completely converted ploidy from hyperdiploidy to hypertetraploidy (accounting for 18.2% of 11 tested bone samples). **(C)** Fully maintained hypertetraploidy of lung metastases formed by LM2-hyper (accounting for 100% of 4 tested lung samples). **(D)** Fully maintained hypertetraploidy of bone metastases formed by BM1-hyper (accounting for 100% of 2 tested bone samples). Legend at the bottom shows signs representing different ploidy peaks of human or mouse origin. N=haploidy of MDA-MB-231.

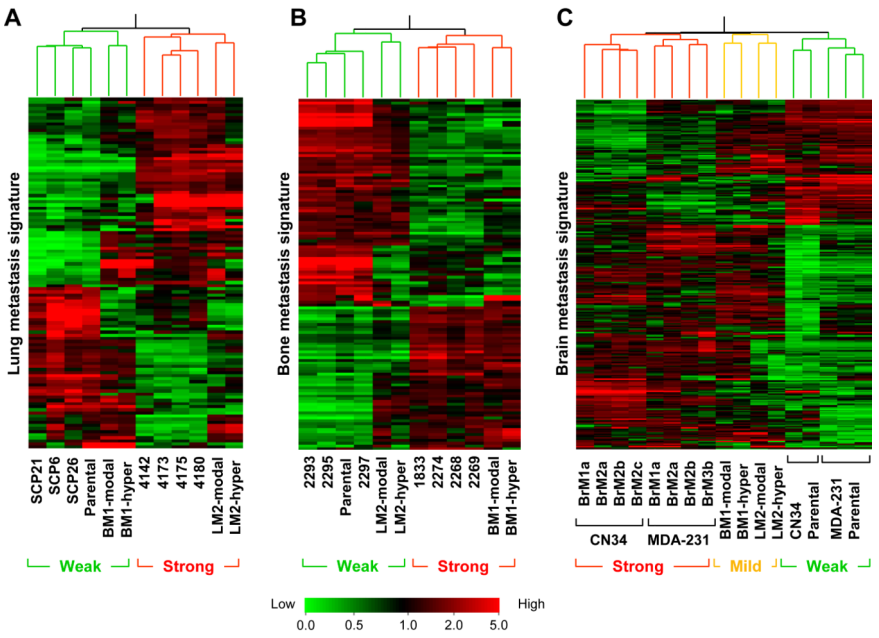

Figure 6.

Modal and hyper cells maintain closely matched expression profile of organ-specific metastasis genes. **(A)** Lung metastasis signature [16] clustering BM1-modal and BM1-hyper together to the weakly lung-metastatic branch and LM2-modal and LM2-hyper together to the strongly lung-metastatic branch. **(B)** Bone metastasis signature [17] clustering LM2-modal and LM2-hyper together to the weakly bone-metastatic branch and BM1-modal and BM1-hyper together to the strongly bone-metastatic branch. **(C)** Genes correlated with brain metastatic behavior [18] clustering LM2-modal and LM2-hyper together, and BM1-modal and BM1-hyper together, to the mildly brain-metastatic branch. In all dendrograms, colors code for metastatic ability: red, strong; orange, mild; green, weak.

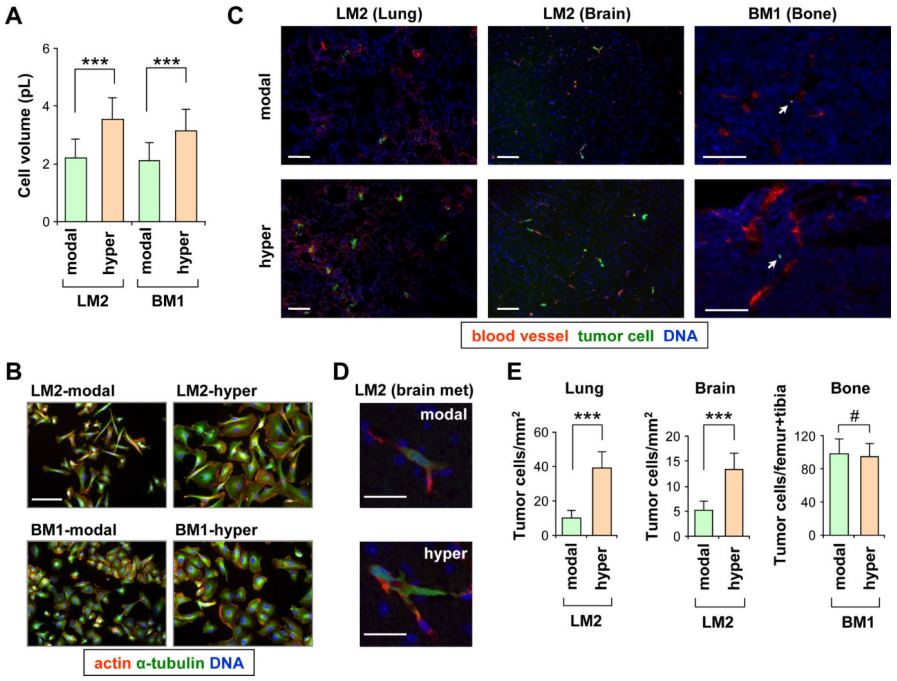

Figure 7.

Enlarged cell size by ploidy duplication caused more cell arrest in the capillary beds in lung and brain, but not in bone. **(A)** Volume of cells in suspension measured with Coulter counter. Error bar represents s.e.m. of 3 independent measurements, (***) $P<0.001$ with Student's t-test. **(B)** Cells in 2D culture stained for actin with palloidin (red), α-tubulin with antibody (green) and DNA with DAPI (blue). **(C)** Tumor cells (green, Cell Tracer labeled) lodging in different organs within 24h post-injection. Capillaries were stained with Texas Red dextran (red) and DNA with DAPI (blue). The few tumor cells in bone marrow were indicated by arrows. **(D)** High resolution image of an LM2-modal cell or an LM2-hyper cell arrested in capillaries in the brain, with same color coding as in **C**. **(E)** Significantly increased tumor cell arrest in lung and brain and similar infiltration in bone. Error bar represents s.d. n=4 mice/group. (***) $P<0.001$ (#) $P > 0.5$ with Student's t-test. Scale bar represents 100μm in **B** and **C**, 25μm in **D**.